Magnetic MoS_2 Interface Monolayer on a CdS Nanowire by Cation Exchange

Chih-Shan Tan[†], **Yu-Jung Lu**[‡], **Chun-Chi Chen**[§], **Pei-Hsuan Liu**[†], **Shangjr Gwo**[‡], **Guang-Yu Guo**[*,∥,⊥], and **Lih-Juann Chen**[*,†]

[†] Department of Materials Science and Engineering, National Tsing Hua University, Hsinchu, Taiwan 30043, R.O.C.

[‡] Department of Physics, National Tsing Hua University, Hsinchu, Taiwan 30043, R.O.C.

[§] National Nano Device Laboratories, National Applied Research Laboratories, 26, Prosperity Road I, Hsinchu, Taiwan 30078, R.O.C.

[∥] Department of Physics, National Taiwan University, Taipei, Taiwan 10617, R.O.C.

[⊥] Physics Division, National Center for Theoretical Sciences, Hsinchu, Taiwan 30078, R.O.C.

J. Phys. Chem. C, **2016**, *120* (40), pp 23055–23060

DOI: 10.1021/acs.jpcc.6b07679

Publication Date (Web): October 3, 2016

*E-mail: gyguo@phys.ntu.edu.tw., *E-mail: ljchen@mx.nthu.edu.tw.

Abstract

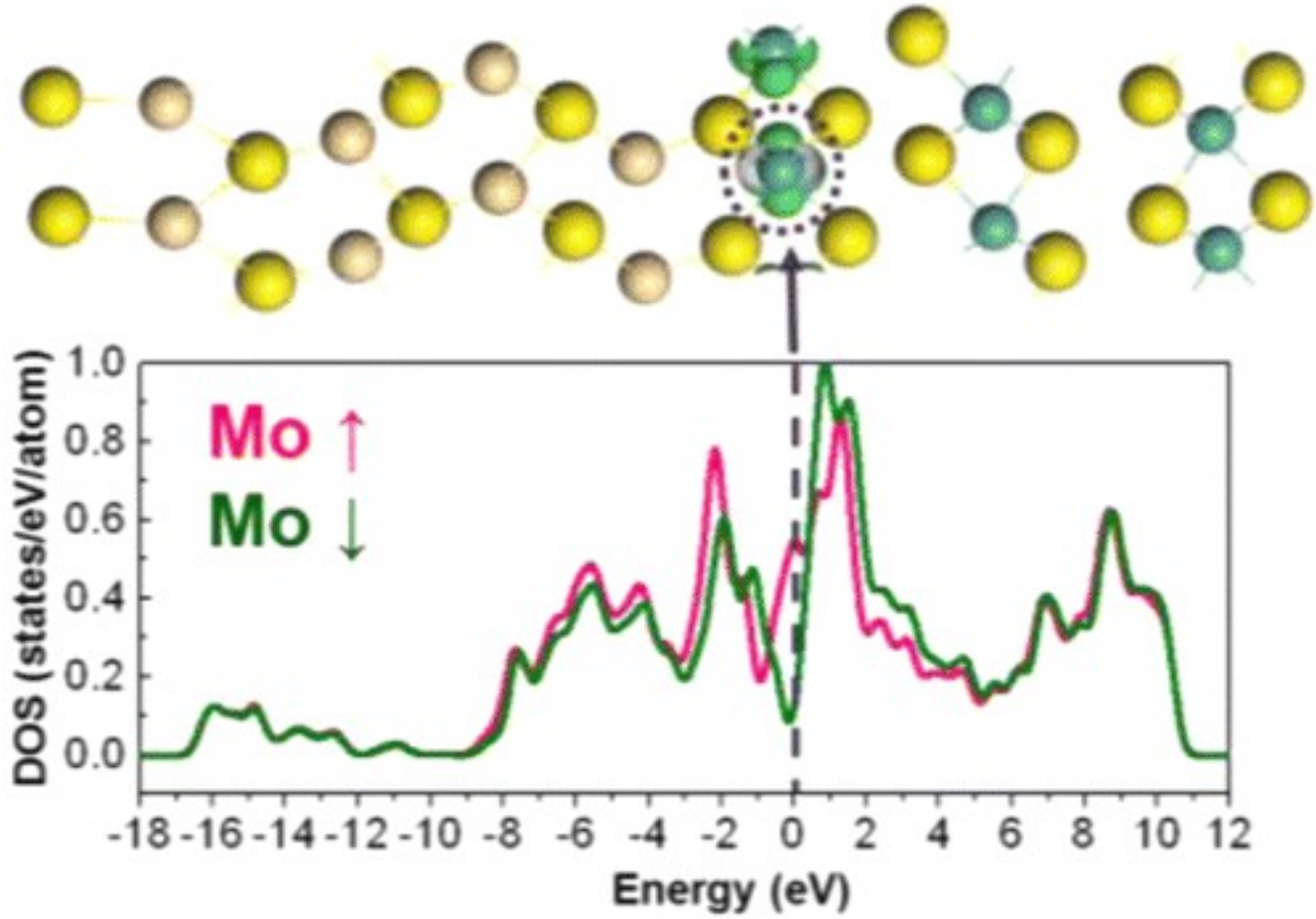

MoS_2 atomic layers have recently attracted much interest because of their two-dimensional structure as well as tunable optical, electrical, and mechanical properties for next-generation electronic and electro-optical devices. Here we have achieved facile fabrication of MoS_2 thin films on CdS nanowires by cation exchange in solution at room temperature and importantly observed their extraordinary magnetic properties. We establish the atomic structure of the MoS_2/CdS heterostructure by taking atomic images of the MoS_2/CdS interface as well as performing first-principles density functional geometry optimizations and scanning transmission electron microscopy annular dark field image simulations. Furthermore, our first-principles density functional calculations for the MoS_2/CdS heterostructure reveal that the magnetism in the MoS_2/CdS heterostructure stems from the ferromagnetic MoS_2 monolayer next to the MoS_2/CdS interface. The ferromagnetism is attributed to the partial occupation of the Mo $d_{x^2-y^2}/d_{xy}$conduction band in the interfacial MoS_2 monolayer caused by the mixed covalent–ionic bonding among the MoS_2 and CdS monolayers near the MoS_2/CdS interface. These findings of the ferromagnetic MoS_2 monolayer with large spin polarization at the MoS_2/semiconductor interface suggest a new route for fabrication of the transition

metal dichalcogenide-based magnetic semiconductor multilayers for applications in spintronic devices.

Introduction

Transition metal dichalcogenide (TMD) monolayers,(1-4) especially those of molybdenum disulfide (MoS_2),(5-8) have recently attracted much interest because of their controllable optical, electrical, and mechanical properties for next-generation devices. Bulk MoS_2 consists of sandwichlike S–Mo–S monolayers in which each Mo atom is connected to six S atoms with covalent bonds. The sandwich MoS_2 monolayers are bound together by weak van der Waals forces. The band structure of MoS_2 undergoes a remarkable change from an indirect band gap of ∼1.2 eV in the bulk to a direct one of ∼1.8 eV for a single monolayer.(9) MoS_2 nanowires exhibit excellent electrochemical performance in lithium ion batteries.(10) Recent researches have been focused on the excellent optical and electrical properties of MoS_2, and some are also related to the novel magnetic properties of MoS_2. For example, it has been reported that the valley magnetic moment of the MoS_2 monolayer could be electrically tuned(11) and that zigzag and armchair nanoribbons of MoS_2 could exhibit metallic (ferromagnetic) and semiconducting (nonmagnetic) behavior.(12-15) It has also been predicted that large spin polarization could be induced in the interfacial MoS_2monolayer in the ferromagnetic Fe_4N/MoS_2 bilayer because of the magnetic proximity effect.(16)Spintronic devices are being developed with vigorous efforts,(17, 18) and a spin transistor(5, 19, 20) is believed to be the most promising next-generation spintronic device.

Although a large amount of research has been directed at the formation of MoS_2 films with atomic thickness, scarce attention has been paid to the process of formation of MoS_2 films and the bonding and physical properties of the MoS_2 layer with other semiconductor materials. Here we use cation exchange to grow epitaxial MoS_2 layers on the surface of CdS nanowires (NWs) at room temperature. Remarkably, we discover that the MoS_2/CdS heterostructures are ferromagnetic. Our first-principles density functional calculations reveal that the magnetism originates from the MoS_2 monolayer at the MoS_2/CdS interface with a spin magnetic moment of ∼0.5 μ_B on the Mo atom and a large spin polarization (∼63%) of the electronic states at the Fermi level. The occurrence of magnetization in the interfacial MoS_2 monolayer is attributed to the Mo cation sharing of its d electron with the Cd cation. As MoS_2 is considered to be an excellent material for transistors,(5) the findings presented here of the itinerant magnetism in the MoS_2monolayer at the MoS_2/semiconductor

interface may reveal a new opportunity for the fabrication of the magnetic two-dimensional (2D) TMD materials on three-dimensional (3D) nanostructures for application in spin transistors and other semiconductor spintronic devices.

Experimental and Computational Methods

CdS NW Synthesis

CdS NWs were grown by using the method reported in ref 21.

Cation Exchange Transformation

CdS NWs were dipped into ethylene glycol (99.5%, Sigma-Aldrich) containing 0.1 M molybdenum(V) chloride (Alfa Aesar, 99.6%) at room temperature. After 6 h, the CdS NWs completely transformed into MoS_2 NWs. We can change the MoS_2 shell thickness by varying the reaction time.

Instrumentation

FE-SEM images were obtained using a FEI Helios 1200^+ FE-SEM instrument. TEM images were recorded using JEOL ARM200F and 2010F electron microscopes. Raman measurements were taken with a Horiba Jobin Yvon, LABRAM HR 800 UV instrument. The magnetic measurements were taken using a SQUID instrument (MPMS XL-7).

Scanning Transmission Electron Microscopy (STEM) Image Simulations

Scanning transmission electron microscopy annular dark field (STEM-ADF) image simulations of the model MoS_2/CdS heterostructures were performed with QSTEM.(22) The input parameters were set according to our experimental conditions, including the probe size, the convergence angle, and the acceptance angle of the ADF detector. To enhance the contrast of the sulfur atoms, the medium-range ADF mode was selected instead of the high-angle ADF mode by proper adjustment of the camera length. The detector angle is at a pivot condition (with 20–60 mrad) between the medium-range ADF mode and the high-angle ADF mode.

Density Functional Calculations

Several initial atomic models of the MoS_2/CdS heterostructure were constructed by different combinations of MoS_2 $(002\bar{1})$ and CdS (002) thin layers. First-principles geometry optimizations for these initial atomic models of the MoS_2/CdS heterostructure were performed on the basis of density functional theory (DFT) with the generalized gradient approximation (GGA) of the Perdew–Burke–Ernzerhof form.(23) The optimized MoS_2/CdS heterostructure models were then used to simulate the STEM-ADF image. The atomic model that produces the image best fitting to the real STEM-ADF

image is displayed in Figure 1, and also used in the subsequent GGA calculations of the electronic and magnetic properties of the MoS_2/CdS heterostructure. First-principles DFT-GGA calculations were performed by using the plane wave norm conserving pseudopotential method, as implemented in the Cambridge Serial Total Energy Package (CASTEP). The plane wave basis set cutoff energy is 720 eV. We used a fine k-point mesh of 5 × 8 × 1 for the Brillouin zone integration throughout.

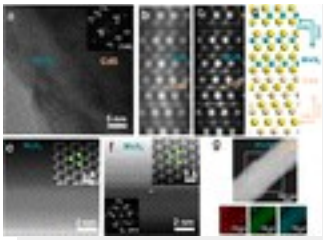

Figure 1. Heterojunction area analysis of MoS_2/CdS NWs after cation exchange. (a) High-resolution TEM image of the MoS_2/CdS heterostructure at the junction area (after reaction for 3 min). The inset is the corresponding FFT pattern. (b) STEM-ADF image of the MoS_2/CdS heterostructure (after reaction for 3 min). (c) Simulated STEM-ADF image of the MoS_2/CdS heterostructure. (d) Atomic model of the MoS_2/CdS junction. (e) STEM-ADF image of the MoS_2 region (after reaction for 3 min). The top right inset is the magnified image of panel e. (f) STEM-ABF image of the MoS_2 region (after reaction for 3 min). The top right and bottom left insets are the magnified image and FFT pattern, respectively. The blue and yellow dots represent Mo and S atoms, respectively. (g) STEM image and EDS mapping of CdS NW after Mo ion exchange for 10 min.

Results and Discussion

Cation exchange is an ionic reaction process for III–V and II–VI semiconductors and metal–organic frameworks for changing the components and structures(24-26) as well as a convenient method for fabricating optical and electrical devices.(27) In a previous work, ion exchange was used to convert CdS nanowire templates to Cu_2S/Ag_2S superlattice p/n heterojunction NWs due to ionic bonding preferences between the different cation and anion.(21) In the work presented here, MoS_2 layers were grown on CdS nanowires by cation exchange and the magnetic properties of MoS_2 (shell)/CdS (core) NWs were explored. CdS NWs were dipped in a molybdenum ionic solution at room temperature (RT), and atomic layers of MoS_2 were grown on CdS NWs. By control of the reaction time, different thicknesses, from one atomic layer to tens of atomic layers, of MoS_2 can be grown on CdS NW as a shell by cation exchange. Finally, the CdS NWs were completely transformed to MoS_2 NWs after several hours.

The ex situ Raman spectra of cation exchange from CdS NWs to MoS_2 NWs with different reaction times of up to 6 h were monitored. Via identification of the E_{2g}^1 (in-plane vibration) and A_{1g} (out of plane) peaks, the gradual formation of MoS_2 structure with increasing reaction time can be inferred (Figure S1 and ref 28). The data exhibit clearly the 302 cm^{-1} peak, which is the first-order longitudinal optical mode (1LO) of CdS. After cation exchange, the CdS 1LO peak shifts gradually with strain and eventually disappears. On the other hand, the magnitudes of E_{2g}^1 and A_{1g} signals of MoS_2 increase gradually. It is difficult to identify the actual location of the E_{2g}^1 peak at 376 cm^{-1} near the CdS peaks until the completion of the reaction. The A_{1g} peaks during the cation exchange from CdS to MoS_2 NWs are at 408 cm^{-1} (2 min), 405 cm^{-1} (3 min), 407 cm^{-1} (4 min), 407 cm^{-1} (5 min), 405 cm^{-1} (10 min), 407 cm^{-1} (30 min), 407 cm^{-1} (1 h), 406 cm^{-1} (2 h), and 406 cm^{-1} (6 h). It indicates that the stress and strain are varied with reaction time and MoS_2thickness. SEM images are shown in Figure S2.

Bright field transmission electron microscopy (BF-TEM) and scanning transmission electron microscopy–energy dispersive spectroscopy (STEM–EDS) were performed to obtain structural information about the MoS_2/CdS interface. We analyzed the MoS_2 on the CdS NW surface after cation exchange reaction for 3–10 min by BF-TEM (Figure 1a). After STEM imaging and EDS mapping of Mo, Cd, and S (Figure 1g), the core–shell structure of CdS-MoS_2 is evident. The scanning transmission electron microscopy annular dark field (STEM-ADF) image (Figure 1b) further reveals that MoS_2 $(00\bar{2})$ is connected with CdS (002) (Figure 1b). The STEM-ADF image matches rather well with the simulated image (Figure 1c) using the atomic model described below (Figure 1d). We built many atomic models for the MoS_2/CdS heterostructure and then performed first-principles geometry optimization calculations for these models that were used in the STEM-ADF image simulations by QSTEM.(22) The MoS_2/CdS heterostructure shown in Figure 1d is the heterostructure model with the simulated STEM-ADF image (Figure 1c) fitted best to the real STEM-ADF image (Figure 1b). From the STEM-ADF (Figure 1e) and ABF (Figure 1f) images, with magnified images as insets, the hexagonal structure of MoS_2 along the [001] direction is evident. Both CdS and MoS_2 are of a hexagonal closely packed (hcp) crystal structure with different lattice parameters. For CdS, $a = b = 0.413$ nm and $c = 0.671$ nm. For MoS_2, $a = b = 0.316$ nm and $c = 1.229$ nm. Consequently, for growth of $(00\bar{2})$ MoS_2 on (002) CdS, the lattice mismatch between CdS and MoS_2 would be as high as 23%. On the other hand, no dislocations were observed at the interface. The absence of misfit dislocations is attributed to the difficulty in nucleation of dislocations in nanostructures.(29, 30)

The hysteresis loops of CdS NWs and MoS_2/CdS NWs have been obtained by a superconducting quantum interference device (SQUID) (Figure 2a–c and Figure S2) with different cation exchange

time (3 s, 6 s, 9 s, 12 s, 1 min, 5 min, 10 min, 30 min, 60 min, 2 h, and 6 h). After cation exchange for 6 h, CdS NWs (M_s = 1.135 × 10^{-3} emu/g, and $H_{c\perp}$ = 215.8 Oe) transform completely to MoS_2NWs (M_s = 5.53 × 10^{-3} emu/g, and $H_{c\perp}$ = 149.9 Oe), and both of them are ferromagnetic. Obviously, growth for 1 min of MoS_2 on CdS NWs leads to the strongest saturation magnetization intensity. In addition, the low-temperature (T = 4 K) hysteresis loop shows a coercivity ($H_{c\perp}$ = 973 Oe) and saturation magnetization intensity (M_s = 4.43 × 10^{-2} emu/g) (Figure S3) higher than the coercivity ($H_{c\perp}$ = 200 Oe) and saturation magnetization intensity (M_s = 1.3 × 10^{-2} emu/g) at room temperature. Figure 2d reveals that the M_s decreases with MoS_2 thickness.

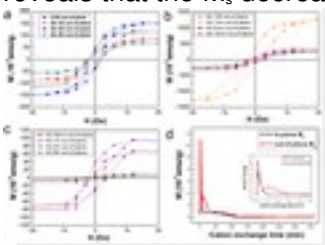

Figure 2. Magnetic measurements of MoS_2/CdS NWs. (a–c) Hysteresis loops of CdS NWs and MoS_2/CdS NWs in the out-of-plane direction. M is magnetization, and H is applied field. (d) Saturation magnetization of MoS_2/CdS NWs as a function of cation exchange time.

For further exploration of the origin and nature of the observed magnetization (M), the knowledge of the electronic structure and atom-resolved magnetization in the MoS_2/CdS heterostructure is essential. Therefore, we have performed self-consistent spin-polarized electronic structure calculations within the DFT-GGA.(23) The atomic model shown in Figure 1d, which generates the simulated STEM-ADF image (Figure 1c) that fits best to the real STEM ADF image (Figure 1b), has been used in the DFT-GGA calculation.

A previous DFT-GGA calculation shows that free-standing few-layer thin films of MoS_2 have no magnetic moment.(31) In contrast, this calculation shows that the MoS_2 monolayer next to the CdS substrate becomes ferromagnetic with a Mo magnetic moment (m_s) of ∼0.5 μ_B and a large electronic state spin polarization (P) of ∼63% at the Fermi level (Figure 3d). Spin polarization $P = (N_\uparrow - N_\downarrow)/(N_\uparrow + N_\downarrow)$, where $N_\uparrow$ and $N_\downarrow$ are the spin-up and spin-down densities of states (DOSs) at the Fermi level (EF), respectively. The Mo magnetic moment and spin polarization are greatly reduced in the second (m_s = 0.01 μ_B, and P = 15%) and third (m_s = 0.00 μ_B, and P = 2%) monolayers of MoS_2 away from the interface, as demonstrated by the calculated Mo-decomposed spin-resolved densities of states (DOSs) displayed in Figure 3d (and also Figure S5). Experimentally, the thinner MoS_2 layers are observed to possess a higher magnetization (M_s), and this is consistent with the results of the

DFT calculation. Clearly, both experimental data and DFT calculation indicate that the interfacial MoS_2 layer has the predominant contribution to the MoS_2/CdS magnetic properties.

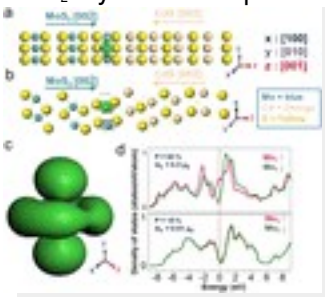

Figure 3. Atomic structure and DFT calculation of the magnetic property of the MoS_2/CdS heterostructure. Atomic models of the MoS_2/CdS heterostructure with MoS_2 $(00\bar{2})$ connecting with CdS (002) along (a) [010] and (b) [110] zone axes. The calculated spin density is concentrated at the first layer of Mo atoms from the junction. (c) Shape (isosurface) of the spin density of the Mo atom on the interfacial MoS_2 monolayer. (d) Spin-resolved DOSs of the Mo atoms on the first and second layers of the interface (top and bottom panels). The red dashed line indicates the Fermi level.

The observed dependence of magnetization on the thickness of the MoS_2 layer on the CdS NW is consistent with the theoretical finding of the magnetism in the MoS_2 monolayer at the MoS_2/CdS interface as revealed by our atomic model (Figures 1d and 3a). Raman peaks (E_{2g}^1 and A_{1g}) of the MoS_2 layer (Figure S1) are clearly seen after cation exchange for 2 min, indicating that the quality of the MoS_2 structure improves as the thickness increases. Indeed, our Raman results show that our MoS_2 layer has a fine 2D structure on the CdS NW with clear in-plane and out-of-plane vibration modes. This explains that the few-layer thick MoS_2 structures have a poor magnetic property. For example, for very few-layer thick MoS_2 films on CdS NWs [3 s (0.5 layer), 6 s (1 layer), 9 s (1.5 layers), and 12 s (2 layers)], the M_s values are lower than that for 5 nm (reaction for 5 min) thick MoS_2 on CdS NWs. For MoS_2 with an improved structure, the interfacial magnetism starts to dominate the magnetic properties. On the other hand, for MoS_2 shells of >5 nm on CdS NWs, the influence of the interfacial magnetism is weakened. As a result, the magnetization decreases with an increase in MoS_2 thickness. Overall, as the CdS NW gradually transforms to the MoS_2 NW, the maximal magnetization moment (M_{max} or M_s) increases first sharply with the formation of a thin shell of MoS_2 and then decreases rapidly. This phenomenon is similar to the variation of the photoluminescence intensity of MoS_2 with thickness.(32)Furthermore, the magnetic force microscopy (MFM) data also show that the magnetic property of MoS_2 depends on the number of layers.(33) The calculated spin density distribution in the MoS_2/CdS heterostructure is exhibited in panels a and b of Figure 3, and that of the Mo atom in the interfacial MoS_2 monolayer is displayed in Figure 3c.

Clearly, there is significant spin density only in the interfacial MoS_2 monolayer (Figure 3a,b), where the spin density distribution of Mo is similar to that of the $d_{x^2-y^2}$ orbital (Figure 3c). The results indicate that the major contribution comes from Mo d orbitals. This is because the Fermi level is raised above the bottom of the conduction Mo $d_{x^2-y^2}$ and d_{xy} bands in the interfacial monolayer, as revealed by calculated Mo-decomposed spin-resolved DOSs shown in Figure 3d (see also Figure S5). Interestingly, the calculated spin-resolved DOS curves show that the local DOS of the Cd atoms on the interfacial Cd monolayer is also spin-polarized (Figure S6), because of the magnetic proximity effect on the Cd atoms by the magnetic Mo atoms via the S atoms across the interface. For example, the spin polarizations for the S atoms on the interface S monolayer and the Cd atoms on the Cd monolayer next to the interface are 20% (S_{M1}) and 16% (Cd_1), respectively (see Figure 4b and also Figures S6 and S7).

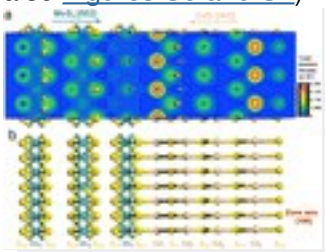

Figure 4. Electron density distribution of the MoS_2/CdS heterostructure. (a) Total electron density distribution of the MoS_2/CdS heterostructure shown with the isosurface (blue line, isovalue of 0.13876 e/Å^3). (b) Atomic model of the MoS_2/CdS heterostructure with the [100] zone axis.

Figure 4a shows the calculated charge density distribution in the MoS_2/CdS heterostructure as modeled by the atomic model shown in Figure 3b. For the sake of discussion, the different atomic locations in the vicinity of the MoS_2/CdS interface are labeled, as shown in Figure 4b. The charge density distribution in the region from the S_{M4} to Cd_2 atom layer is rather flat, having a similar isosurface with an isovalue of 0.139 e/Å^3. Inside the region, the electron density in some areas is higher than the isovalue, indicating some bonding between the S and Cd atoms across the MoS_2/CdS interface. This covalent bonding could be attributed to the similar electronegativities of the Mo (1.3) and Cd (1.5) atoms. Remarkably, the calculated DOS curves (Figure S5) show that this covalent bonding causes some charge transfer from the Mo d bands in the outer MoS_2monolayer (Mo_3) to the Mo d bands in the interfacial MoS_2 monolayer (Mo_1), leading to the partial occupation of the Mo $d_{x^2-y^2}$ and d_{xy} dominant bands of the Mo_1 atoms. This charge transfer is also seen from the calculated numbers of valence electrons on the Mo_1 (6.38), Mo_2 (6.17), and Mo_3(6.02) atoms (Table S1). As a result, the strong exchange interaction among the Mo d electrons then gives rise to the

formation of the Mo_1 spin magnetic moment, and hence the ferromagnetic MoS_2 monolayer next to the MoS_2/CdS interface.

Conclusions

In summary, magnetic MoS_2 thin films have been grown on CdS NWs by cation exchange at room temperature. The magnetism in the MoS_2/CdS heterostructure was shown to stem from the ferromagnetic MoS_2 monolayer next to the MoS_2/CdS interface by first-principles DFT-GGA calculations. The ferromagnetism was attributed to the partial occupation of the Mo $d_{x^2-y^2}/d_{xy}$ conduction band in the interfacial MoS_2 monolayer caused by the mixed covalent–ionic bonding among the MoS_2 and CdS monolayers near the MoS_2/CdS interface. This work thus offers a new paradigm for fabrication of the transition metal dichalcogenide-based magnetic semiconductor multilayers for applications in spintronic devices such as tunnel junctions with high magnetoresistance.

Supporting Information

The Supporting Information is available free of charge on the ACS Publications website at DOI: 10.1021/acs.jpcc.6b07679.

- Additional figures displaying measured Raman spectra, SEM images and hysteresis loops, and calculated atom- and orbital-decomposed densities of states and additional tables listing calculated occupation numbers of atomic orbitals and structural parameters of the atomic model adopted in the SEM image simulations and DFT-GGA calculations (PDF)

- **PDF**
  - jp6b07679_si_001.pdf (910.93 kB)

Magnetic MoS_2 Interface Monolayer on a CdS Nanowire by Cation Exchange

figshare

ShareDownload

The authors declare no competing financial interest.

Acknowledgment

We thank K. L. Lin at National Nano Device Laboratories for a discussion of the experimental results. The authors are grateful for the research support from the Ministry of Science and Technology of R.O.C. under Projects MOST 103-2221-E-007-003 and MOST 104-2112-M-002-002-MY3, the Academia Sinica Thematic Research Program, and the National Center of Theoretical Sciences.

- Reference QuickView

References

This article references 33 other publications.

1. 1.

   Wang, Q. H.; Kalantar-Zadeh, K.; Kis, A.; Coleman, J. N.; Strano, M. S. Electronics and Optoelectronics of Two-dimensional Transition Metal Dichalcogenides *Nat. Nanotechnol.* **2012**, 7, 699– 712 DOI: 10.1038/nnano.2012.193

   [Crossref], [PubMed], [CAS]

2. 2.

   Johari, P.; Shenoy, V. B. Tuning the Electronic Properties of Semiconducting Transition Metal Dichalcogenides by Applying Mechanical Strains *ACS Nano* **2012**, 6, 5449– 5456 DOI: 10.1021/nn301320r

   [ACS Full Text], [CAS]

3. 3.

   Hong, X.; Liu, J.; Zheng, B.; Huang, X.; Zhang, X.; Tan, C.; Chen, J.; Fan, Z.; Zhang, H. A Universal Method for Preparation of Noble Metal Nanoparticle-decorated Transition Metal Dichalcogenide Nanobelts *Adv. Mater.* **2014**, 26, 6250– 6254 DOI: 10.1002/adma.201402063

   [Crossref], [PubMed], [CAS]

4. 4.

Fang, H.; Tosun, M.; Seol, G.; Chang, T. C.; Takei, K.; Guo, J.; Javey, A. Degenerate n-doping of Few-layer Transition Metal Dichalcogenides by Potassium *Nano Lett.* **2013**, 13, 1991– 1995 DOI: 10.1021/nl400044m

[ACS Full Text], [CAS]

5. 5.

Radisavljevic, B.; Radenovic, A.; Brivio, J.; Giacometti, V.; Kis, A. Single-layer MoS_2 Transistors *Nat. Nanotechnol.* **2011**, 6, 147– 150 DOI: 10.1038/nnano.2010.279

[Crossref], [PubMed], [CAS]

6. 6.

Splendiani, A.; Sun, L.; Zhang, Y.; Li, T.; Kim, J.; Chim, C. Y.; Galli, G.; Wang, F. Emerging Photoluminescence in Monolayer MoS_2 *Nano Lett.* **2010**, 10, 1271– 1275 DOI: 10.1021/nl903868w

[ACS Full Text], [CAS]

7. 7.

Li, Y.; Wang, H.; Xie, L.; Liang, Y.; Hong, G.; Dai, H. MoS_2 Nnanoparticles Grown on Graphene: an Advanced Catalyst for the Hydrogen Evolution Reaction *J. Am. Chem. Soc.* **2011**, 133, 7296– 7299 DOI: 10.1021/ja201269b

[ACS Full Text], [CAS]

8. 8.

Lee, K.; Kim, H. Y.; Lotya, M.; Coleman, J. N.; Kim, G. T.; Duesberg, G. S. Electrical Characteristics of Molybdenum Disulfide Flakes Produced by Liquid Exfoliation *Adv. Mater.* **2011**, 23, 4178– 4182 DOI: 10.1002/adma.201101013

[Crossref], [PubMed], [CAS]

9. 9.

Liu, N.; Kim, P.; Kim, J. H.; Ye, J. H.; Kim, S.; Lee, C. J. Large-area Atomically Thin MoS_2 Nanosheets Prepared Using Electrochemical Exfoliation *ACS Nano* **2014**, 8, 6902– 6910 DOI: 10.1021/nn5016242

[ACS Full Text], [CAS]

10. 10.

Yang, L.; Wang, S.; Mao, J.; Deng, J.; Gao, Q.; Tang, Y.; Schmidt, O. G. Hierarchical MoS_2/polyaniline Nanowires with Excellent Electrochemical Performance for Lithium-ion Batteries *Adv. Mater.* **2013**, 25,1180– 1184 DOI: 10.1002/adma.201203999

[Crossref], [PubMed], [CAS]

11. 11.

Wu, S.; Ross, J. S.; Liu, G.
B.; Aivazian, G.; Jones, A.; Fei, Z.; Zhu, W.; Xiao, D.; Yao, W.; Cobden, D.;Xu, X. Electrical Tuning of Valley Magnetic Moment Through Symmetry Control in Bilayer MoS_2 *Nat. Phys.***2013**, 9, 149– 153 DOI: 10.1038/nphys2524

[Crossref], [CAS]

12. 12.

Li, Y.; Zhou, Z.; Zhang, S.; Chen, Z. MoS_2 nanoribbons: High Stability and Unusual Electronic and Magnetic Properties *J. Am. Chem. Soc.* **2008**, 130, 16739– 16744 DOI: 10.1021/ja805545x

[ACS Full Text], [CAS]

13. 13.

Tongay, S.; Varnoosfaderani, S. S.; Appleton, B. R.; Wu, J.; Hebard, A. F. Magnetic Properties of MoS_2: Existence of Ferromagnetism *Appl. Phys. Lett.* **2012**, 101, 123105 DOI: 10.1063/1.4753797

[Crossref], [CAS]

14. 14.

Zhang, J.; Soon, J. M.; Loh, K. P.; Yin, J.; Ding, J.; Sullivian, M. B.; Wu, P. Magnetic Molybdenum Disulfide Nanosheet Films *Nano Lett.* **2007**, 7, 2370– 2376 DOI: 10.1021/nl071016r

[ACS Full Text], [CAS]

15. 15.

Pan, H.; Zhang, Y. W. Edge-dependent Structural, Electronic and Magnetic Properties of MoS_2 Nanoribbons*J. Mater. Chem.* **2012**, 22, 7280– 7290 DOI: 10.1039/c2jm15906f

[Crossref], [CAS]

16. 16.

Feng, N.; Mi, W.; Cheng, Y.; Guo, Z.; Schwingenschlögl, U.; Bai, H. Magnetism by Interfacial Hybridization and p-type Doping of MoS_2 in Fe_4N/MoS_2 Superlattices: A First-principles Study *ACS Appl. Mater. Interfaces* **2014**, 6, 4587– 4594 DOI: 10.1021/am500754p

[ACS Full Text], [CAS]

17. 17.

Chang, L. T.; Wang, C. Y.; Tang, J.; Nie, T.; Jiang, W.; Chu, C. P.; Arafin, S.; He, L.; Afsal, M.; Chen, L. J.Electric-field Control of Ferromagnetism in Mn-doped ZnO Nanowires *Nano Lett.* **2014**, 14, 1823– 1829DOI: 10.1021/nl404464q

[ACS Full Text], [CAS]

18. 18.

Tang, J.; Wang, C. Y.; Chang, L. T.; Fan, Y.; Nie, T.; Chan, M.; Jiang, W.; Chen, Y. T.; Yang, H. J.;Tuan, H. Y.Electrical Spin Injection and Detection in Mn_5Ge_3/Ge/Mn_5Ge_3 Nanowire Transistors *Nano Lett.* **2013**, 13, 4036– 4043 DOI: 10.1021/nl401238p

[ACS Full Text], [CAS]

19. 19.

Koo, H. C.; Kwon, J. H.; Eom, J.; Chang, J.; Han, S. H.; Johnson, M. Control of Spin Precession in a Spin-injected Field Effect Transistor *Science* **2009**, 325, 1515– 1518 DOI: 10.1126/science.1173667

[Crossref], [PubMed], [CAS]

20. 20.

Chuang, P.; Ho, S. C.; Smith, L. W.; Sfigakis, F.; Pepper, M.; Chen, C. H.; Fan, J. C.; Griffiths, J. P.;Farrer, I.; Beere, H. E.; Jones, G. A. C.; Ritchie, D. A.; Chen, T.-M. All-electric All-semiconductor Spin Field-effect Transistors *Nat. Nanotechnol.* **2014**, 10, 35– 39 DOI: 10.1038/nnano.2014.296

[Crossref], [PubMed]

21. 21.

Tan, C. S.; Hsiao, C. H.; Wang, S. C.; Liu, P. H.; Lu, M. Y.; Huang, M. H.; Ouyang, H.; Chen, L. J. Sequential Cation Exchange Generated Superlattice Nanowires Forming Multiple p–n Heterojunctions *ACS Nano* **2014**,8, 9422– 9426 DOI: 10.1021/nn5035247

[ACS Full Text], [CAS]

22. 22.

Koch, C. T. Determination of Core Structure Periodicity and Point Defect Density Along Dislocations. Ph.D. Thesis, Arizona State University, Tempe, AZ, **2002**.

23. 23.

Perdew, J. P.; Burke, K.; Ernzerhof, M. Generalized Gradient Approximation Made Simple *Phys. Rev. Lett.***1996**, 77, 3865 DOI: 10.1103/PhysRevLett.77.3865

[Crossref], [PubMed], [CAS]

24. 24.

Beberwyck, B. J.; Alivisatos, A. P. Ion Exchange Synthesis of III–V nanocrystals *J. Am. Chem. Soc.* **2012**,134, 19977– 19980 DOI: 10.1021/ja309416c

[ACS Full Text], [CAS]

25. 25.

Gupta, S.; Kershaw, S. V.; Rogach, A. L. Ion Exchange in Colloidal Nanocrystals *Adv. Mater.* **2013**, 25,6923– 6944 DOI: 10.1002/adma.201302400

[Crossref], [PubMed], [CAS]

26. 26.

Kim, M.; Cahill, J. F.; Fei, H.; Prather, K. A.; Cohen, S. M. Postsynthetic Ligand and Cation Exchange in Robust Metal–organic Frameworks *J. Am. Chem. Soc.* **2012**, 134, 18082– 18088 DOI: 10.1021/ja3079219

[ACS Full Text], [CAS]

27. 27.

Tang, J.; Huo, Z.; Brittman, S.; Gao, H.; Yang, P. Solution-processed Core-shell Nanowires for Efficient Photovoltaic Cells *Nat. Nanotechnol.* **2011**, 6, 568– 572 DOI: 10.1038/nnano.2011.139

[Crossref], [PubMed], [CAS]

28. 28.

Tan, C. S.; Chen, H. Y.; Chen, H. S.; Gwo, S.; Chen, L. J. Intermediates in the Cation Reactions in Solution Probed by an in situ Surface Enhanced Raman Scattering Method *Sci. Rep.* **2015**, 5, 13759 DOI: 10.1038/srep13759

[Crossref], [PubMed], [CAS]

29. 29.

Lu, K. C.; Wu, W. W.; Wu, H. W.; Tanner, C. M.; Chang, J. P.; Chen, L. J.; Tu, K. N. In-situ Control of Atomic-scale Si Layer with Huge Strain in the Nano-heterostructure NiSi/Si/NiSi Through Point Contact Reaction*Nano Lett.* **2007**, 7, 2389– 2394 DOI: 10.1021/nl071046u

[ACS Full Text], [CAS]

30. 30.

Kästner, G.; Goesele, U. Stress and Dislocations at Cross-sectional Heterojunctions in a Cylindrical Nanowire *Philos. Mag.* **2004**, 84, 3803– 3824 DOI: 10.1080/14786430420002813 89

[Crossref]

31. 31.

Wang, C. Y.; Guo, G. Y. Nonlinear Optical Properties of Transition Metal Dichalcogenide MX_2 (M= Mo, W; X= S, Se) Monolayers and Trilayers from First-principles Calculations *J. Phys. Chem. C* **2015**, 119, 13268–13276 DOI: 10.1021/acs.jpcc.5b01866

[ACS Full Text]

32. 32.

Li, H.; Zhang, Q.; Yap, C. C. R.; Tay, B. K.; Edwin, T. H. T.; Olivier, A.; Baillargeat, D. From Bulk to Monolayer MoS_2: Evolution of Raman Scattering *Adv. Funct. Mater.* **2012**, 22, 1385– 1390 DOI: 10.1002/adfm.201102111

[Crossref], [CAS]

33. 33.

Li, H.; Qi, X.; Wu, J.; Zeng, Z.; Wei, J.; Zhang, H. Investigation of MoS_2 and Graphene Nanosheets by Magnetic Force Microscopy *ACS Nano* **2013**, 7, 2842– 2849 DOI: 10.1021/nn400443u

[ACS Full Text], [CAS]